



# Antibacterial and Antiproliferative Effect of ZnO Nanoparticles Prepared Using *Origanum marjorana* Plant and *Garcinia indica* Fruit extracts

Guddappa Halligudra<sup>1,2</sup> · Lakshmi Sourabha K J<sup>1</sup> · Vinaya K<sup>3</sup> · Navya Rani M<sup>4</sup> · Dinesh Rangappa<sup>1</sup> · Prasanna Daddakunche Shivaramu<sup>1</sup>

Received: 31 July 2024 / Accepted: 17 August 2024

© The Author(s), under exclusive licence to Springer Science+Business Media, LLC, part of Springer Nature 2024

## Abstract

In the present study, the aqueous seed extract of an *Origanum marjorana* plant and the fruit rind extract of a *Garcinia indica* plant were used to prepare ZnO nanoparticles. The antimicrobial effects of the prepared nanoparticles on bacterial pathogens and their antiproliferative effects on the HCT 116 cancer cell line were evaluated, with a specific focus on colon cancer. The prepared ZnO nanoparticles were characterized via XRD, SEM, FTIR, and UV–Vis spectroscopy. The antibacterial activities of the synthesized nanoparticles were studied against both the gram-positive and gram-negative microorganisms *B. cereus* and *S. typhi*. These compounds presented moderate activity compared with the standard ciprofloxacin. The MICs for OM-ZnO were 2 µg/mL for *S. typhi* and 2 µg/mL for *B. cereus*. For GI-ZnO, 4 µg/mL for *S. typhi* and 4 µg/mL for *B. cereus* were observed. These results confirmed that the antibacterial efficacy of the nanoparticles depends on their concentration. The antiproliferative effects of the ZnO nanoparticles were evaluated using the MTT assay and cell cycle analysis. ZnO nanoparticles showed good antiproliferative effects on the tested cell lines. Studies on the cell cycle have suggested that ZnO nanoparticles effectively induce cell cycle arrest at the G2/M phase and trigger apoptosis. Compared with untreated HCT 116 cells (9.31%), those treated with 80 and 160 µg/mL ZnO nanoparticles arrested 25.92% and 33.57%, respectively, at the G2/M phase of the cell cycle. This study effectively demonstrates the synthesis of ZnO nanoparticles using plant extracts, highlighting their antimicrobial and antiproliferative properties. The detailed characterization underscores their potential for applications in antimicrobial therapies and cancer treatment.

**Keywords** Green extracts · ZnO nanoparticles · Antibacterial activity · Antiproliferative activity

## 1 Introduction

Nanoscience and technology are rapidly growing research avenues with various engineering applications in numerous sectors, such as mechatronics, electrochemistry, optics, energy conservation, biotechnology, pharmaceuticals, and food [1–5]. Various techniques have been utilized to modify and reduce inorganic materials to the nanoscale for technical and scientific purposes. In recent years, significant progress has been achieved in nanoparticle research, leading to the availability of excellent methods and tools for creating nanoparticles of desired size and shape. These advancements provide specific requirements, aiming to obtain improved properties and functionalities [6, 7]. Currently, the synthesis of nanoparticles through biological methods and plant extracts has gained popularity among researchers

✉ Prasanna Daddakunche Shivaramu  
prasuds@gmail.com; prasannads@vtu.ac.in

<sup>1</sup> Department of Applied Sciences, Visvesvaraya Technological University, Muddenahalli Campus, Chikkaballapur, Karnataka 562101, India

<sup>2</sup> Department of Chemistry, ATME College of Engineering, Mysuru, Karnataka 570028, India

<sup>3</sup> Department of Chemistry, I.D.S.G. Government College, Chikkamagaluru, Karnataka 577102, India

<sup>4</sup> Center for Research & Development, Nagarjuna College of Engineering and Technology (NCET), Bengaluru, Karnataka, India

due to their ability to be synthesized in ambient atmosphere, cost-effectiveness, environmental adaptability, low toxicity, and facile application [8]. The resulting particles are easily dispersible in water, making them eco-friendly, with no need for additional toxic stabilizers [9–11]. The high surface area and reactivity of nanoparticles make them suitable for therapeutic applications in various dosage forms and administration routes [12, 13]. Different types of metals, metal oxides, or sulfide nanoparticles can be prepared from various biogenic sources, including microbes, plant extracts, and enzyme [14–22].

Zinc oxide (ZnO) nanoparticles are wurtzite structures composed of a wide bandgap semiconductor that can easily absorb UV radiation and significantly increase the binding energy [23]. These materials are synthesized using various methods and from a variety of plant sources. ZnO nanoparticles have been utilized in the production of food packaging materials, and various methods and materials for integrating ZnO into these products have been described [9, 23–26]. ZnO is widely recognized as safe by the U.S. Food and Drug Administration and is commonly referred to as GRAS [27]. Scientific investigations have shown that zinc deficiency in cells can initiate and promote cancer, whereas excess zinc can have detrimental effects [28]. In addition to these essential uses, ZnO and other nanoparticles are employed for various applications, such as solar cells, optoelectronics, piezoelectrics, photocatalysis, spintronics, infrared reflectivity, biosensors, drug/gene delivery, antioxidants, antimicrobials, antiarthritics, and cytotoxic applications [29–35].

Owing to increasing concerns about the rise in antibiotic resistance caused by pathogenic microorganisms, there is a need to develop materials that can function as effective antimicrobial agents. Moreover, nanoparticles synthesized using green methods can self-functionalize molecular drugs on their surface, leading to an enhanced antibacterial effect [36–38]. Cancer is characterized by the uncontrolled growth of a mass of cells that tend to proliferate uncontrollably and, in some instances, metastasize [39]. The surface properties of ZnO nanoparticles enable potential interaction with biomolecules, which can be utilized to target active cancer sites or to attach chemotherapeutic agents, thereby improving their efficacy [40, 41].

Numerous studies have explored the antibacterial and antiproliferative properties of ZnO nanoparticles produced from various medicinal plant extracts [42–44]. These nanoparticles have been extensively studied for their ability to inhibit and kill major foodborne pathogens, such as *Escherichia coli* and *Staphylococcus aureus*, at designated doses [45–48]. Additionally, these nanoparticles have demonstrated strong antibacterial effects against human pathogens such as *Pseudomonas aeruginosa*, *Staphylococcus aureus*, and *Enterococcus faecalis*. Several studies on these

nanoparticles have investigated their antimicrobial activity against *bacteria* isolated from peppermint leaf extract and frozen ice cream [49, 50]. Therefore, the specific mechanism of the antibacterial action of these nanoparticles is still under investigation [49, 51, 52]. Moreover, these nanoparticle properties have been linked to decreased microbial enzyme activity, reactive oxygen species production, cell membrane damage, and genotoxic effects [53–55]. Current obstacles in the synthesis of ZnO nanoparticles from *Origanum marjorana* (OM) and *Garcinia indica* (GI) extracts include improving the extraction methods and elucidating the effects of various factors on the dimensions, morphology, and stability of the synthesized nanoparticles [56–59]. Furthermore, ensuring the reproducibility and scalability of the synthesis process is crucial for potential industrial applications. Addressing these challenges will contribute to the development of an efficient and reliable method for producing zinc oxide nanoparticles with improved antibacterial and antiproliferative properties [55].

Considering these points, in continuation of our efforts to develop various nanoparticles for various applications [60–67], the present research involved synthesizing ZnO nanoparticles from traditional and folkloric OM and GI plants in a convenient way. The plant-assisted synthesis of ZnO nanoparticles is safe and involves the use of a wide variety of metabolites or phytochemicals that may act as capping and stabilizing agents. OM, known as Marwa in India, has retained medicinal and therapeutic properties and is also used as a functional food for humans [68]. It consists of antiseptic, antispasmodic, carminative, stimulant, expectorant, and nerve tonic remedies and functions as a cure for asthma, cough, indigestion, rheumatism, dyspepsia, flatulence, toothache, and heart conditions [69, 70]. Kokum (GI) is an important indigenous tree that is recognized by several names, including *Bindin*, *Bhinda*, and *Kokum*. The dried rind of the fruit is used primarily as an acidulate in cosmetic products for the treatment of piles, dysentery, tumors, and heart complaints [71–73]. While there is abundant information available on the antimicrobial properties of ZnO against various microorganisms, this research specifically examined the inhibitory effects of ZnO nanoparticles on cell growth and the antibacterial properties of these materials using eco-friendly resources. This research presents the synthesis of zinc oxide nanoparticles using leaf extracts from OM and fruit rind extracts from GI. The nanoparticles were analyzed using various techniques, such as X-ray diffraction (XRD), scanning electron microscopy (SEM), Fourier transform infrared spectroscopy (FTIR), and UV–visible spectroscopy. Additionally, this study explored the antimicrobial and antiproliferative properties of zinc oxide nanoparticles to assess their potential applications.

## 2 Experimental

### 2.1 Materials and Methods

All chemicals and reagents used were of analytical grade and were used without any further purification. Deionized water (DI-H<sub>2</sub>O) from Millipore Milli-Q Systems was used throughout the experiment. The following chemicals and reagents were sourced from the indicated suppliers with their respective purities: zinc nitrate hexahydrate (Sigma Aldrich, 98%), dimethyl sulfoxide (Sigma Aldrich, 99.9%), ethanol (Sigma Aldrich, 99.9%), propidium iodide (Sigma Aldrich, ≥95%), (3-[4,5-dimethylthiazol-2-yl]-2,5-diphenyl tetrazolium bromide) (Sigma Aldrich, 98%), soybean casein digest agar (Thermo Fisher Scientific, >98%), Dulbecco's modified Eagle's medium (Thermo Fisher Scientific, >98%), tryptone broth (Thermo Fisher Scientific, >99%), and phosphate-buffered saline (Sigma Aldrich, 99.9%).

### 2.2 Preparation of Plant Extracts

GI fruit rinds were procured from a local market, washed with DI-H<sub>2</sub>O to remove dust and then shade-dried under ambient conditions. The dehydrated fruit rind was crushed, sieved and stored in ambient room conditions. 10 g of powder was mixed with DI-H<sub>2</sub>O (200 mL) and then heated at 80 °C for 30 min. After completion, the resulting mixture was filtered and stored for further use. Similarly, OM leaves were collected, rinsed with running water to remove dust, rinsed with DI-H<sub>2</sub>O and allowed to dry at room temperature. The dried leaves were then powdered, sieved and stored. The same procedure was used to obtain fruit extracts from the rinds Figure 1.

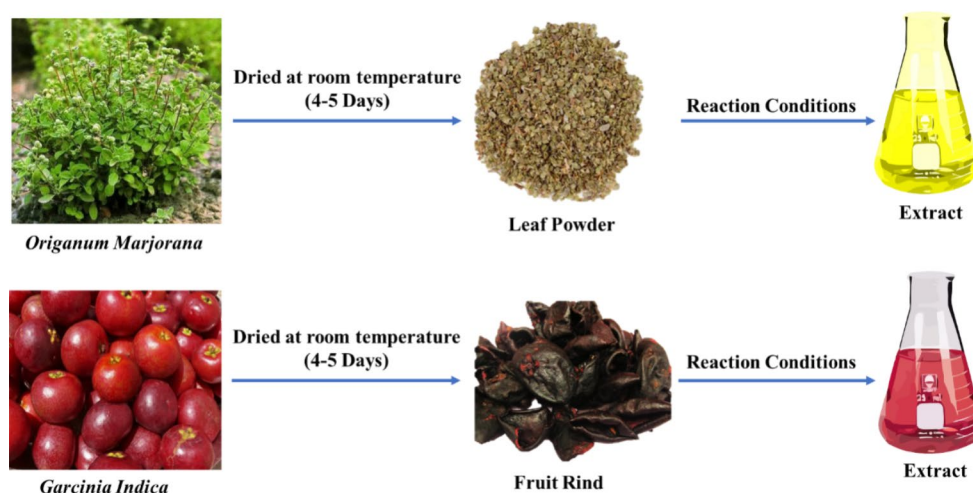
### 2.3 Synthesis of ZnO Nanoparticles

ZnO nanoparticles were synthesized by combining 10 mL of leaf extract and/or rind extract with 50 mL of 0.05 M zinc nitrate solution. The resulting solution was heated at 80 °C for 30 min with constant stirring. The appearance of white particles confirmed the formation of the nanoparticles. Subsequently, these nanoparticles were separated by centrifugation, dried, and calcined in a muffle furnace at 300 ± 10 °C for 2 h to produce white ZnO nanoparticles. To ensure their stability, the synthesized ZnO nanoparticles were characterized for their structural integrity and consistency over time, confirming their robustness in subsequent analyses Figure 2.

### 2.4 Characterization of the Nanoparticles

The synthesized nanoparticles were characterized using various analytical techniques. XRD was employed to identify the crystal structure of the prepared nanomaterials, providing details on the average spacing between atomic layers, the orientation, size, and shape of single crystals, and the internal stress of small crystalline regions. In this study, XRD analysis was conducted using a Rigaku Ultima-IV instrument with a wavelength of 0.15406 nm and a nickel filter at a scan speed of 2° min<sup>-1</sup>. For surface morphology analysis, a Hitachi (SEM Model SU1510) was utilized. A FT-IR spectrophotometer (Spectrum Two, PerkinElmer System) was employed to identify the functional groups of the sample within the 4000–400 cm<sup>-1</sup> region. To investigate the interactions between ultraviolet or visible electromagnetic radiation and the sample, a Perkin-Elmer Lambda 750 spectrophotometer was utilized.

**Fig. 1** Schematic diagrams of the preparation of OM leaf and GI fruit rind extracts



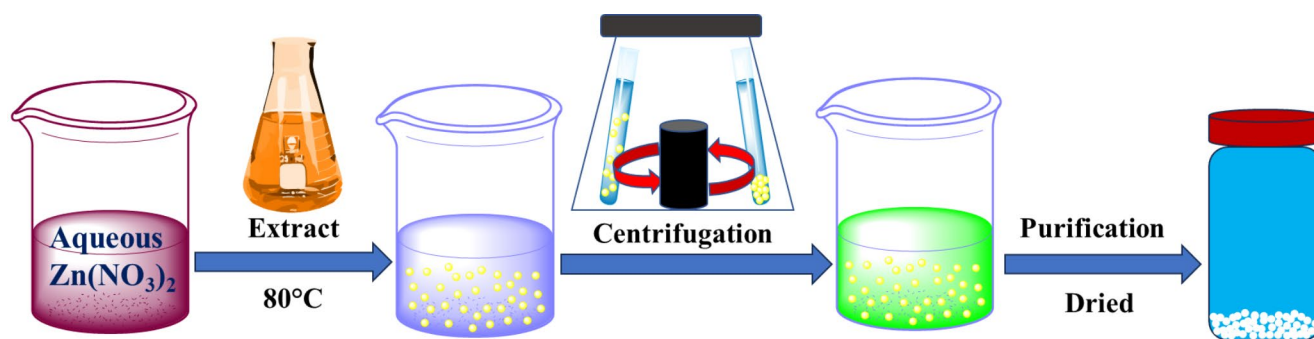


Fig. 2 Schematic diagram of the green-mediated synthesis of ZnO nanoparticles and analysis of the nanoparticles

## 2.5 Antimicrobial Activity

Bacterial cultures were prepared by suspending cells obtained from cultures that were subsequently grown in tryptone broth, and the concentrations were adjusted to  $1-2 \times 10^5$  cells/mL.

## 2.6 Agar-well Diffusion Method

Various concentrations of ZnO nanoparticles have been used against different bacterial species. For instance, *Bacillus cereus* and *Salmonella typhi* were targeted using this method. Following agar well diffusion, the medium was prepared by pouring 20 mL of Soyabean casein digest agar (SCDA) onto Petri dishes. The mixture was then allowed to solidify and seeded with a 24 h culture of the bacterial strains. Agar wells with a diameter of 5 mm were created using sterile Pasteur pipettes, and 20  $\mu$ L of the test sample was added to each well. The plates were incubated at 37 °C for 24 h to enable the samples to diffuse and interact with the medium. The resulting zone of inhibition, identified by a uniform circular area with dense growth, was measured in millimeters. Ciprofloxacin was used as the positive control [36].

## 2.7 Minimum Inhibitory Concentration (MIC)

Dilution susceptibility testing mechanisms are adopted to determine the minimal inhibitory concentration of antimicrobial agents needed to inhibit gram-positive *Bacillus cereus* and gram-negative *Salmonella typhi*. This can be achieved by diluting antimicrobial agents in agar or broth media. Tryptone broth (90  $\mu$ L) was added to the 96-well plate at different concentrations, and a 1 mg/mL sample was added and serially diluted (twofold dilutions). Afterward, 10  $\mu$ L of the sample was added to each well, excluding the control, and the mixture was then incubated at 37 °C for 24 h.

## 2.8 Cytotoxicity Studies Using the HCT 116 Cell Line by MTT Assay

The human colon cancer cell line HCT-116, obtained from the American Type Culture Collection (Manassas, U.S.), was utilized for the research studies. In this method, 70–80% of the confluent cells were assessed for viability and subsequently centrifuged. Approximately 50,000 cells were seeded in each well of a clean 96-well plate and then incubated with 5% CO<sub>2</sub> at 37 °C for 24 h. ZnO nanoparticles were then added to Dulbecco's modified Eagle medium (DMEM) without fetal bovine serum (FBS) at concentrations ranging from 0 to 320  $\mu$ g/mL and cultured for 24 h. Subsequently, 100  $\mu$ L of MTT reagent (5 mg/10 mL of MTT in 1X PBS) was added to the wells, and the cells were cultured for 3–4 h. The reagent was then removed and replaced with 100  $\mu$ L of DMSO was added rapidly to solubilize the formazan. Then in order to take reading the absorbance was measured at 590 nm [74].

## 2.9 Cell Characterization by Flow Cytometry

The percentages of cells in different phases of the cell cycle and the percentages of cells treated with or without ZnO nanoparticles were determined using FACS Caliber (BD Biosciences, San Jose, CA). The cells were seeded for 48 h and then exposed to ZnO nanoparticles. A total of  $1 \times 10^6$  cells were placed in 6-well plates with 2 mL of complete DMEM and incubated at 37 °C with 5% CO<sub>2</sub> for 24 h. The cells were then exposed to either 80 or 160 mg/mL ZnO nanoparticles, with 1% DMSO serving as the control. Later, the cells were collected, centrifuged to collect pellets, and resuspended gently in 1X PBS. The cells were fixed overnight with 2 mL of fixing solution (70% ethanol). The pellet was rinsed twice with 2 mL of chilled 1X PBS and subsequently exposed to 500  $\mu$ L of propidium iodide (PI) solution, which included 0.05 mg/mL PI and 0.05 mg/mL RNase in PBS, for 15 min at room temperature [75].

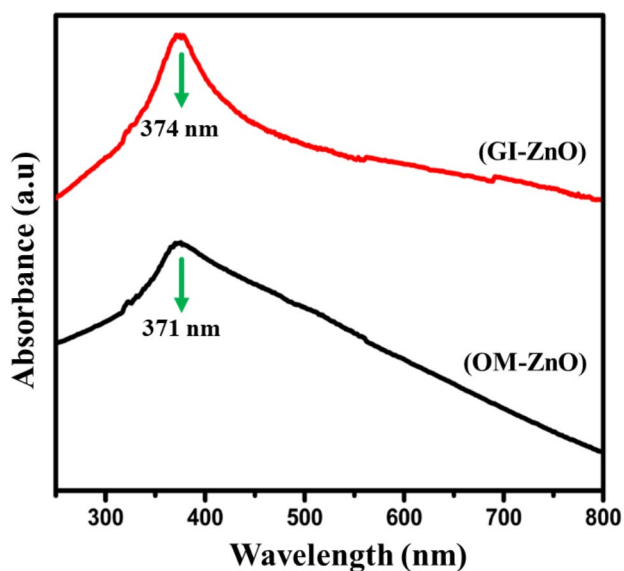


Fig. 3 UV-Vis spectra of the OM-ZnO and GI-ZnO nanoparticles

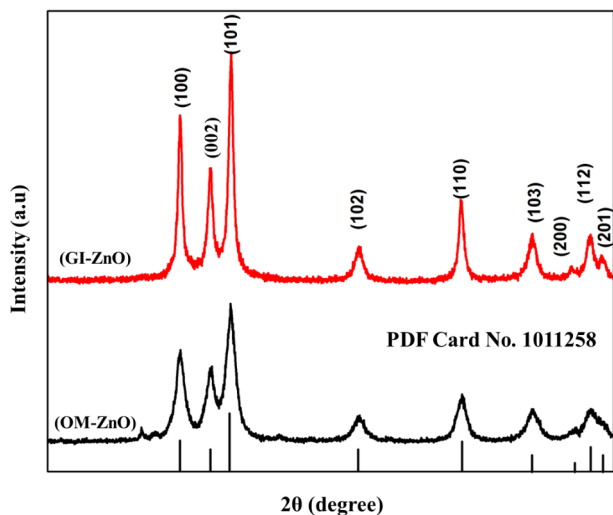


Fig. 4 XRD patterns of the OM-ZnO and GI-ZnO nanoparticles

### 3 Results and Discussions

#### 3.1 Spectroscopic Characterization of the Prepared Nanoparticles

UV-Vis spectroscopy was used to analyze the optical characteristics of the ZnO nanoparticles synthesized from extracts of OM (OM-ZnO) and GI (GI-ZnO). Figure 3 displays distinct peaks at 371 nm for OM-ZnO and 374 nm for GI-ZnO in the UV-vis spectra, indicating the characteristic absorption of the ZnO nanoparticles. The slight shift in the absorption peaks between OM-ZnO and GI-ZnO suggested variances in the size or shape of the nanoparticles

produced using different plant extracts. These absorption peaks are consistent with the typical absorption range for ZnO nanoparticles, confirming the successful synthesis of nanoparticles using OM and GI extracts as reducing and capping agents, respectively. The optical properties of ZnO nanoparticles are crucial for potential applications, as absorption peaks can reveal their size and structure. XRD and SEM analysis can provide additional characterization of the crystalline structure and morphology. OM-ZnO and GI-ZnO nanoparticles exhibit distinctive optical properties associated with the extracts of OM and GI. Variations in optical properties may affect antibacterial and antiproliferative activities, highlighting the need for further research to gain a comprehensive understanding of these processes.

XRD analysis was conducted at 40 kV and 30 mA, with patterns recorded between  $10^\circ$  and  $70^\circ$  at a scanning rate of  $2^\circ$  per second. The distinctive peaks observed in the XRD pattern are depicted in Fig. 4. The peaks at  $2\theta$  angles of 32.07, 34.47, 36.53, 47.79, 57.17, 63.10, 67.07, 68.49, and 69.78 were attributed to the (100), (002), (101), (102), (110), (103), (200), (112), and (201) planes, respectively. The obtained XRD results are in good agreement with those previously reported for ZnO nanoparticles. The absence of other non-characteristic/additional peaks clearly demonstrates the purity of the as-synthesized ZnO nanoparticles. The presence of prominent peaks in the (100), (002), and (101) planes indicates that the ZnO nanoparticles are highly crystalline and in a single phase. These data revealed that the sample had a wurtzite crystal structure with space group P6<sub>3</sub>/mc belonging to a hexagonal lattice system (DB card no. 1011258), and the presence of peaks corresponding to ZnO nanoparticles was verified [76]. This confirmed that crystalline ZnO nanoparticles were formed from the plant extracts using an environmentally friendly synthesis method. The wurtzite crystallite sizes of OM-ZnO and GI-ZnO were calculated via the Debye-Scherrer equation and were found to be 12.76 and 14.11 nm, respectively.

FTIR tests were conducted to identify the functional groups responsible for capping and stabilizing the synthesized metal oxide nanoparticles. The FTIR spectra for OM-ZnO and GI-ZnO are illustrated in Fig. 5. The stretching of Zn-O was observed at approximately  $480\text{ cm}^{-1}$ . The peak at  $864\text{ cm}^{-1}$  indicates the stretching vibrations of the alkane groups. The peaks at  $1594$  and  $1403\text{ cm}^{-1}$  correspond to the C=O stretch in the aromatic ring and the C=C stretch in the polyphenols, respectively. At  $3378\text{ cm}^{-1}$ , the O-H stretching vibrations may be attributed to external moisture. The peak at  $872\text{ cm}^{-1}$  in the GI-ZnO spectra indicates the C-H stretching vibrations of the alkane groups. The  $1118\text{ cm}^{-1}$  peak represents the C-O stretching vibration of the amino acid. The peak at  $1479\text{ cm}^{-1}$  represents the C=C bond, corresponding to vibrations in protein amide linkages.

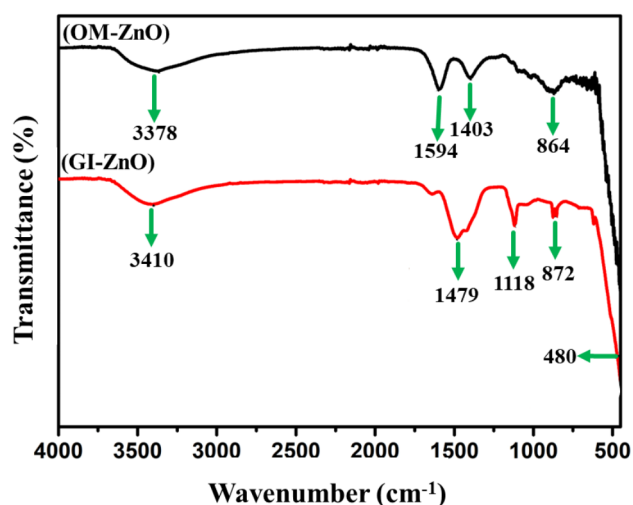
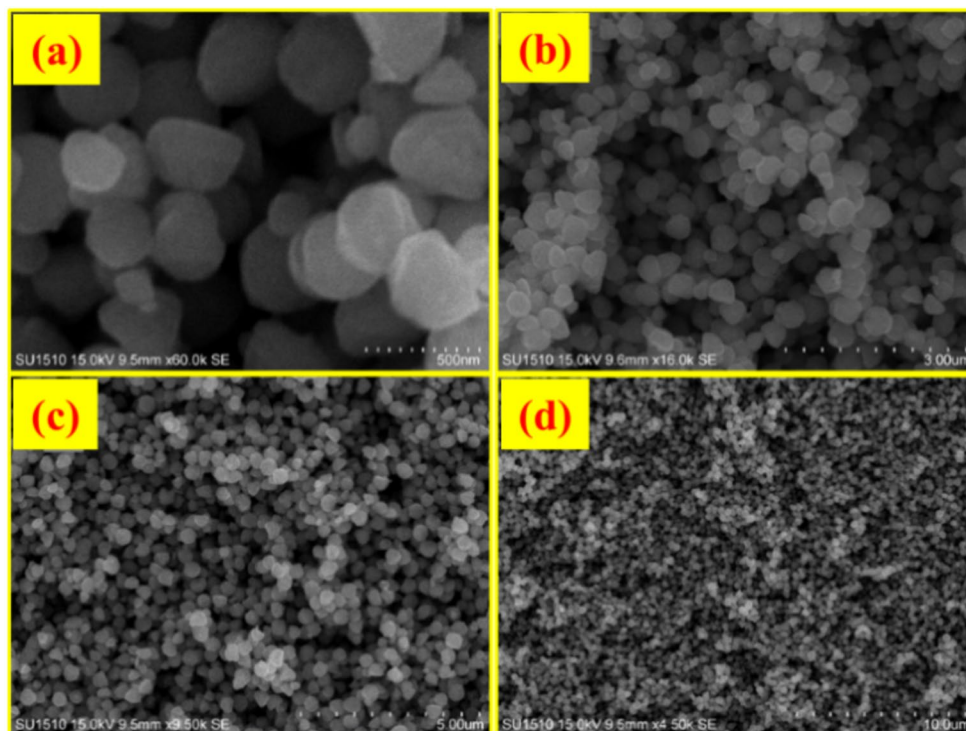


Fig. 5 FTIR spectra of OM-ZnO and GI-ZnO nanoparticles

Therefore, the synthesized OM-ZnO and GI-ZnO nanoparticles were able to form and stabilize the ZnO nanoparticles.

To examine the surface morphology of the nanoparticles, SEM studies were conducted. SEM images of the ZnO (OM and GI) nanocrystalline particles are shown in Figs. 6 and 7. These images, captured at various magnifications (500 nm, 3  $\mu\text{m}$ , 5  $\mu\text{m}$ , and 10  $\mu\text{m}$ ), indicate that the particles are polydispersed with various sizes and are almost spherical in shape. The green synthesis method used to produce ZnO nanoparticles was found to be effective at achieving a uniform distribution of nanoparticles ranging in size

Fig. 6 SEM images of OM-ZnO nanoparticles



from 20 to 50 nm without any agglomeration. The smaller size and significantly larger surface area of the particles, which are attached to prominent phytochemicals, enabled them to develop a morphology with a uniform distribution. The elements in the sample could be identified by the peaks obtained for the ZnO nanoparticles using EDX. EDX plots of the ZnO nanoparticles obtained through SEM are included in supplementary information Figures (S1 and S2), which shows the presence of zinc (Zn) and oxygen (O) present in the samples.

### 3.2 Biological Applications of the Prepared ZnO Nanoparticles

#### 3.2.1 Antibacterial Activity Determination by the Well Diffusion Method

The antibacterial activity of the plant and fruit extracts of the ZnO nanoparticles was determined using the well diffusion method. The synthesized ZnO nanoparticles were tested against both gram-positive (*B. cereus*) and gram-negative (*S. typhi*) bacteria. The zone of inhibition around each well was measured by calculating the diameter of the inhibition zone (mm). The resulting inhibition zones for OM-ZnO were 10 mm for *S. typhi* and 11 mm for *B. cereus*. GI-ZnO exhibited an 11 mm zone for *S. typhi* and an 8 mm zone for *B. cereus* (Table 1). Figure 8 illustrates a clear inhibition zone after treatment with ZnO nanoparticles compared to treatment with the standard antibiotic ciprofloxacin.

**Fig. 7** SEM images of GI-ZnO nanoparticles

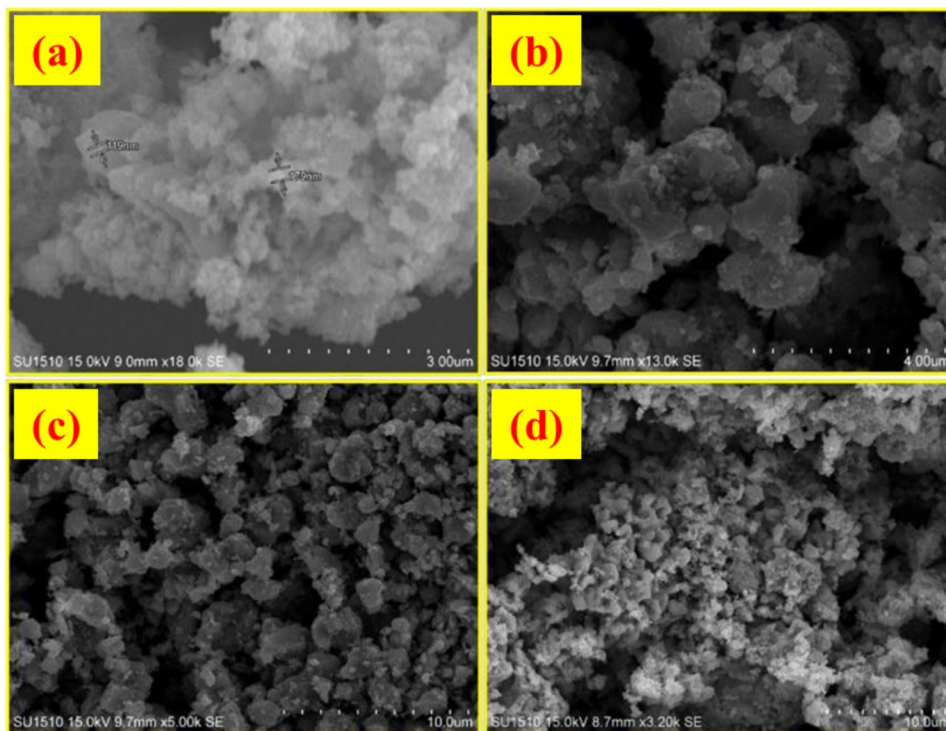


**Table 1** Zone of inhibition obtained by well diffusion method

Sl. No	Test Organisms	OM-ZnO in (mm)	GI-ZnO in(mm)	Standard (Ciprofloxacin)
1	<i>S. Typhi</i>	10	11	21
2	<i>B. cereus</i>	11	8	21

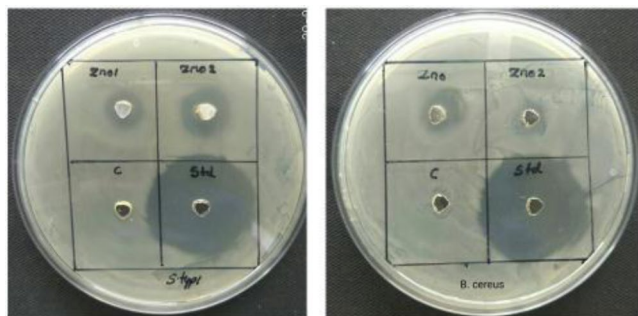
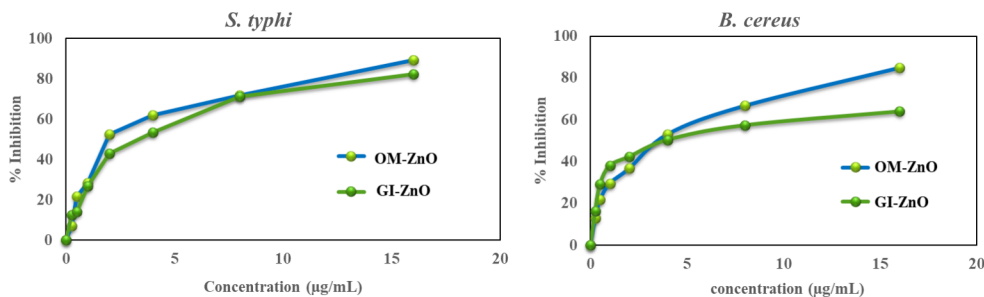


**Fig. 8** Zone of inhibition of the OM-ZnO and GI-ZnO nanoparticles

**Fig. 9** Percentages of *S. typhi* and *B. cereus* inhibited by ZnO nanoparticles



### 3.2.2 Determination of the Minimum Inhibitory Concentration Against Pathogenic Bacteria

The minimum inhibitory concentration (MIC) of different concentrations of ZnO nanoparticles was determined against both gram-positive (*B. cereus*) and gram-negative (*S. typhi*) bacteria. The MIC is the minimum concentration of the drug that resulted in 50% inhibition of the absorbance of the ZnO nanoparticles. This was determined using a 96-well microplate at 590 nm, measured in a Tecan plate reader after 24 h of incubation with the standard strain. Figure 9 illustrates that as the absorbance decreased, the number of attached cells also decreased. The MICs for OM-ZnO were 2 µg/mL for *S. typhi* and 2 µg/mL for *B. cereus*; for GI-ZnO, 4 µg/mL for *S. typhi* and 4 µg/mL for *B. cereus* were observed.

**Fig. 10** Cytotoxic effects of ZnO nanoparticles on HCT 116 cells and Calu-6 cells

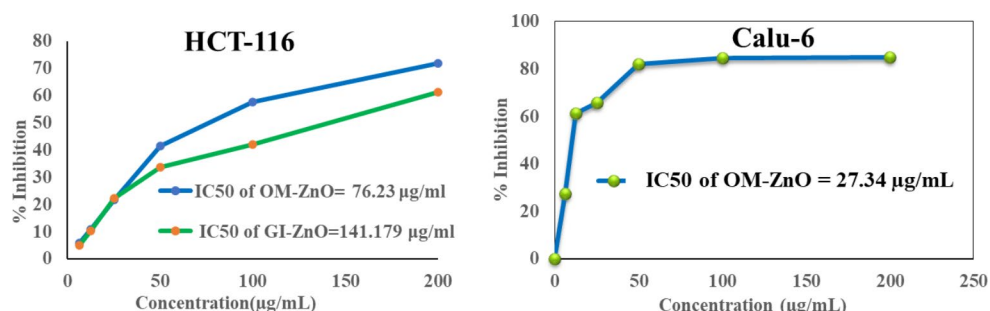
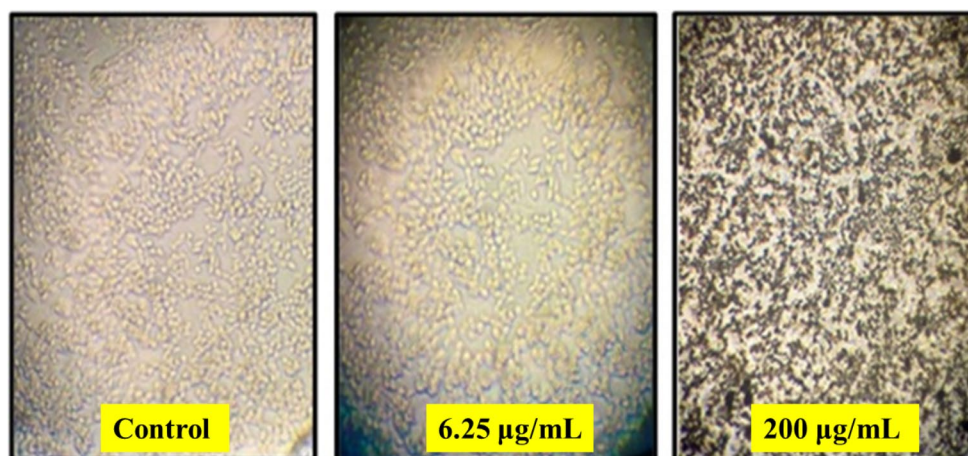


**Fig. 11** Cell viability of the OM-ZnO nanoparticles



### 3.2.3 Cytotoxic Effects of the ZnO Nanoparticles Determined by the MTT Assay

HCT116 cells were exposed to ZnO nanoparticles at concentrations ranging from 6.25 to 200 µg/mL and Calu-6 cells were exposed to concentrations ranging from 10 to 200 µg/mL for 24 h. As the concentrations of ZnO nanoparticles increased, cell viability decreased. The prepared OM-ZnO and GI-ZnO nanoparticles hindered the growth of HCT 116 cells, with IC<sub>50</sub> values of 76.23 and 141.17 µg/mL, respectively. Additionally, OM-ZnO exhibited cytotoxicity on Calu-6 cells, with an IC<sub>50</sub> value of 27.34 µg/mL, as illustrated in Fig. 10. These results indicate that the synthesized ZnO nanoparticles have cytotoxic effects and impede the proliferation of cancer cells in a concentration-dependent manner. In Fig. 11, untreated HCT116 cells displayed an epithelial morphology, while ZnO nanoparticle-treated cells showed significant morphological alterations, losing their characteristic epithelial-like appearance. These pronounced morphological changes indicated the loss of contact with neighboring cells, accompanied by a noticeable reduction in cell size.

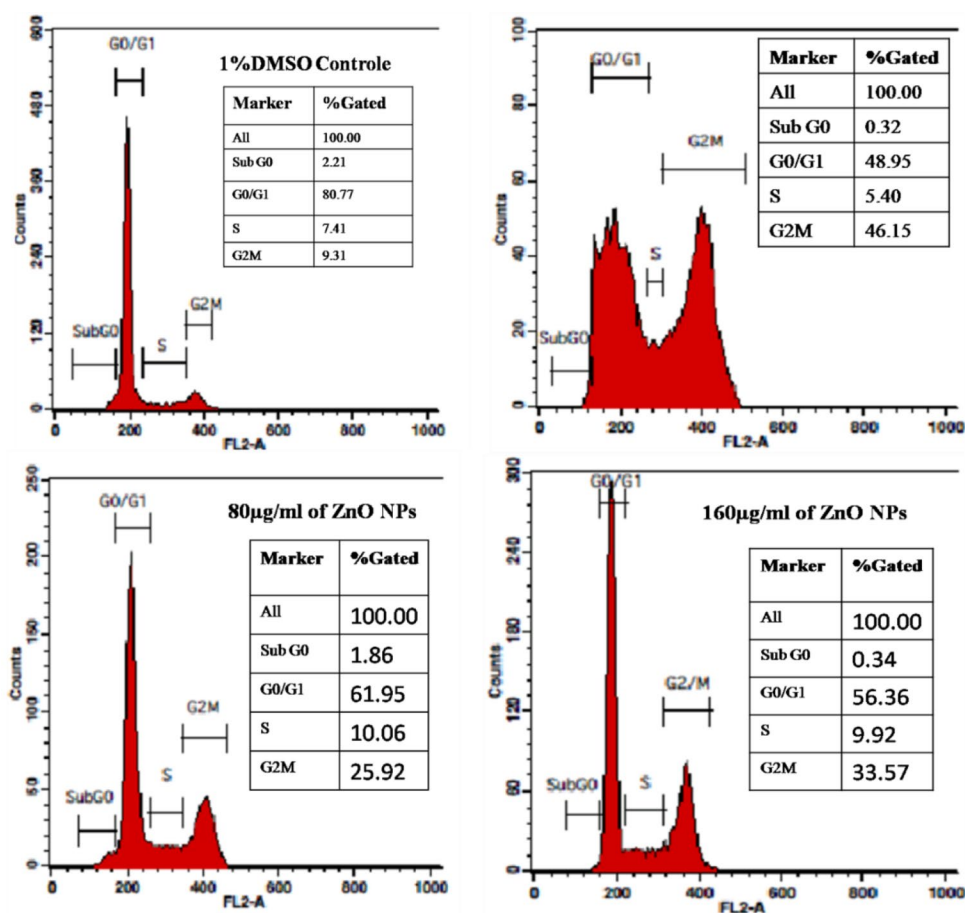
### 3.2.4 Cell Cycle Analysis by FACS

Cell cycle studies were performed on OM-ZnO and GI-ZnO nanoparticles. The cells were treated with apoptosis-inducing

agents, leading to a subpopulation of cells in each subcell due to endonuclease activation and subsequent DNA leakage. Necrotic cells do not show an immediate reduction in DNA content, allowing for the distinction between apoptotic and necrotic cells. Figure 12 illustrates a dose-dependent G<sub>2</sub>/M cell cycle arrest in HCT116 cells treated with ZnO nanoparticles. Treatment with ZnO nanoparticles at 80 and 160 µg/mL resulted in 25.92% and 33.57% cell cycle arrest, respectively, at the G<sub>2</sub>/M phase compared to untreated HCT116 cells (9.31%). Colchicine treatment arrested 46.15% of the cells in the G<sub>2</sub>/M phase. These results suggest that the ZnO nanoparticle extract effectively promotes cell cycle arrest at the G<sub>2</sub>/M phase and simultaneously induces apoptosis.

## 4 Conclusion

ZnO nanoparticles synthesized from *Origanum marjorana* and *Garcinia indica* extracts were characterized using XRD, SEM, FTIR, and UV-Vis spectroscopy. The XRD patterns indicated a wurtzite structure with crystallite sizes of 12.76 nm for OM-ZnO and 14.11 nm for GI-ZnO. SEM images revealed spherical nanoparticles with agglomeration. The FT-IR spectra confirmed the presence of different functional groups and Zn-O bond stretching. The UV-Vis spectra of the prepared ZnO nanoparticles revealed absorption peaks at 371 nm for the OM-ZnO nanoparticles and

**Fig. 12** FACS analysis of the OM-ZnO nanoparticles

at 374 nm for the GI-ZnO nanoparticles. The antibacterial activities of the synthesized nanoparticles showed moderate activity when compared with the standard ciprofloxacin. The MICs for OM-ZnO were 2 µg/mL for *S. typhi* and 2 µg/mL for *B. cereus*. For GI-ZnO, 4 µg/mL for *S. typhi* and 4 µg/mL for *B. cereus* were observed. The prepared OM-ZnO and GI-ZnO nanoparticles exhibited cytotoxic effects by inhibiting the growth of HCT 116 cells, with IC<sub>50</sub> values of 76.23 µg/mL and 141.17 µg/mL, respectively. Treatment with ZnO nanoparticles at concentrations of 80 and 160 µg/mL arrested 25.92% and 33.57%, respectively, of the cancer cells in the G2/M phase of the cell cycle. The synthesized ZnO nanoparticles from *Origanum marjorana* and *Garcinia indica* extracts have significant potential for application as antibacterial agents, anticancer treatments, sensors, catalysts, and photocatalysts. Further research and development in these areas could lead to practical applications in various biomedical and industrial sectors.

**Supplementary Information** The online version contains supplementary material available at <https://doi.org/10.1007/s10904-024-03349-0>.

**Acknowledgements** PDS thanks the Science and Engineering Research Board, Department of Science and Technology, Government of India, for the SIRE Fellowship (SIR/2022/001321).

**Author Contributions** GH: methodology, data curation, Writing-original draft, review & editing. LSJ: Investigation; Methodology; Data curation, Formal analysis. VK: Writing review & editing. NR: Writing review & editing. DR: Resources; Supervision; Writing - review & editing. PDS: Resources, Conceptualization, Supervision, Writing - review & editing.

**Data Availability** No datasets were generated or analysed during the current study.

## Declarations

**Competing Interests** The authors declare no competing interests.

## References

1. S. Malik, K. Muhammad, Y. Waheed, *Molecules* **28**, (2023)
2. S.S. Salem, E.N. Hammad, A.A. Mohamed, and W. El-Dougoud, *Biointerface Res Appl Chem* **13**, (2023)
3. A.S. El-Kalliny, M.S. Abdel-Wahed, A.A. El-Zahhar, I.A. Hamza, and T. A. Gad-Allah, *Discover Nano* **18**, (2023)
4. M.M. El-Kady, I. Ansari, C. Arora, N. Rai, S. Soni, D.K. Verma, P. Singh, A.E.D. Mahmoud, *J. Mol. Liq* **370**, (2023)
5. A. Alkaladi, A.M. Abdelazim, M. Afifi, *Int. J. Mol. Sci.* **15**, (2014)
6. F.E. Ettadili, S. Aghris, F. Laghrib, A. Farahi, S. Saqrane, M. Bakasse, S. Lahrich, M.A. El Mhammedi, *J. Mol. Struct.* **1248**, (2022)

7. S. Kazemi, A. Hosseingholian, S.D. Gohari, F. Feirahi, F. Moameri, G. Mesbahian, Z.S. Moghaddam, Q. Ren, *Mater. Today Sustain.* **24**, (2023)
8. C. Chikkanayakanahalli Paramesh, A. Giridasappa, A.K. Channapillekoppalu Siddegowda, D. Rangappa, and P. Doddakunche Shivaramu, in *Silver Nanoparticles for Drug Delivery* (2023)
9. S. Zeghoud, H. Hemmami, B. Ben Seghir, I. Ben Amor, I. Kouadri, A. Rebiai, M. Messaoudi, S. Ahmed, P. Pohl, J. Simal-Gandara, *Mater. Today Commun.* **33**, (2022)
10. L. Xu, Z. Zhu, D.W. Sun, *ACS Nano* **15**, (2021)
11. N. Bala, S. Saha, M. Chakraborty, M. Maiti, S. Das, R. Basu, P. Nandy, *RSC Adv.* **5**, (2015)
12. D. Chenthamara, S. Subramaniam, S.G. Ramakrishnan, S. Krishnaswamy, M.M. Essa, F.H. Lin, M.W. Qoronfleh, *Biomater. Res.* **23**, (2019)
13. H. Zhao, H. Su, A. Ahmeda, Y. Sun, Z. Li, M.M. Zangeneh, M. Nowrozi, A. Zangeneh, R. Moradi, *Appl. Organomet. Chem.* **36**, (2022)
14. K. Ngcongco, S.B.N. Krishna, K. Pillay, *Front. Chem.* **11**, (2023)
15. S.H. Gebre, *J. Clust. Sci.* **34**, (2023)
16. D.S. Chormey, B.T. Zaman, T. Borahan Kustanto, S. Erarpat Bodur, S. Bodur, Z. Tekin, O. Nejati, S. Bakirdere, *Nanoscale.* **15**, 19423 (2023)
17. A. Carrapiço, M.R. Martins, A.T. Caldeira, J. Mirão, L. Dias, *Microorganisms* **11**, (2023)
18. F. Ameen, T. Dawoud, S. AlNadhari, *Environ. Res.* **202**, (2021)
19. D. Indhira, M. Krishnamoorthy, F. Ameen, S.A. Bhat, K. Arumugam, S. Ramalingam, S.R. Priyan, G.S. Kumar, *Environ. Res.* **212**, (2022)
20. G. Wang, A. Ahmeda, Z. Malek, S. Mansooridara, A. Zangeneh, M.M. Zangeneh, *Appl. Organomet. Chem.* **34**, (2020)
21. A. Dehnoee, R. Javad Kalbasi, M.M. Zangeneh, M.R. Delnavazi, A. Zangeneh, *Micro Nano Lett.* **18**, (2023)
22. A. Dehnoee, R. Javad Kalbasi, M.M. Zangeneh, M.R. Delnavazi, A. Zangeneh, *J. Clust. Sci.* **35**, (2024)
23. S. Raha, M. Ahmaruzzaman, *Nanoscale Adv.* **4**, (2022)
24. S. Maher, B. Zamina, M. Riaz, S. Riaz, N. Khalid, M. Imran, S. Fahmid, H. Ishtiaq, S. Parveen, *ACS Omega.* **8**, 46715 (2023)
25. M.A. Subhan, N. Neogi, K.P. Choudhury, *Nanomanufacturing* **2**, (2022)
26. S. Smaoui, I. Chérif, H. Ben Hlima, M.U. Khan, M. Rebezov, M. Thiruvengadam, T. Sarkar, M.A. Shariati, J.M. Lorenzo, *Food Packag. Shelf Life* **36**, (2023)
27. M.A. Mokammel, M.J. Islam, M. Hasanuzzaman, S. Hashmi, in *Ref. Module Mater. Sci. Mater. Eng.* (2019)
28. Y. Zhang, Y. Tian, H. Zhang, B. Xu, H. Chen, *Biomed. Pharmacotherapy* **133**, (2021)
29. Y. Li, N. Li, W. Jiang, G. Ma, M.M. Zangeneh, *Int. J. Biol. Macromol.* **163**, (2020)
30. J. Liu, A. Zangeneh, M.M. Zangeneh, B. Guo, *J. Exp. Nanosci.* **15**, (2020)
31. A. Ahmeda, M.M. Zangeneh, A. Zangeneh, *Appl. Organomet. Chem.* **34**, (2020)
32. L.V. Hublikar, S.V. Ganachari, N. Raghavendra, N.R. Banapurmath, V.B. Patil, T.M. Yunus, Khan, I.A. Badruddin, *Coatings* **11**, (2021)
33. L.V. Hublikar, S.V. Ganachari, V.B. Patil, *Nanoscale Adv.* **5**, (2023)
34. A. Giridasappa, S.M. Ismail, D. Rangappa, G. Shanubhogana-halli Maheshwarappa, N.R. Marilingaiah, S.S.R. Gollapalli, and P. Daddakunche Shivaramu, *Appl. Nanosci.* **11**, 2561 (2021)
35. A. Giridasappa, D. Rangappa, G.S. Maheswarappa, N.R. Marilingaiah, C.K. Thammaiah, I.M. Shareef, R.K. Subbegowda, P.D. Shivaramu, *Appl. Nanosci.* **11**, 1393 (2021)
36. S. Vijayakumar, S. Mahadevan, P. Arulmozhi, S. Sriram, P.K. Praseetha, *Mater. Sci. Semicond. Process.* **82**, (2018)
37. M. Saravanan, V. Gopinath, M.K. Chaurasia, A. Syed, F. Ameen, N. Purushothaman, *Microb. Pathog.* **115**, (2018)
38. A. Khan, T. Kamal, M. Saad, F. Ameen, S.A. Bhat, M.A. Khan, F. Rahman, *Spectrochim. Acta Mol. Biomol. Spectrosc.* **290**, (2023)
39. D. Kebebe, Y. Liu, Y. Wu, M. Vilakhamxay, Z. Liu, J. Li, *Int. J. Nanomed.* **13**, (2018)
40. A. Yusuf, A.R.Z. Almotairy, H. Henidi, O.Y. Alshehri, M.S. Aldughaim, *Polym. (Basel)* **15**, (2023)
41. M. Sangeetha Vidhya, F. Ameen, T. Dawoud, R. Yuvakkumar, G. Ravi, P. Kumar, D. Velauthapillai, *Mater. Lett.* **283**, (2021)
42. I.A. Shaikh, B. Turakani, M.H. Mahnashi, A.S. Alqahtani, S.H. Hariri, M.M. Ghoneim, H.A. Ebrahim, M. El-Sherbiny, B.A. Mannasaheb, U.M. Muddapur, G. Khuwaja, A.A. Khan, S.E. Dafalla, T. Begum, and S. M. Shakeel Iqbal, *J. King Saud Univ. Sci.* **35**, 102957 (2023)
43. Y.H.I. Mohammed, S. Alghamdi, B. Jabbar, D. Marghani, S. Beigh, A.S. Abouzied, N.E. Khalifa, W.M.A. Khojali, B. Huwaimel, D.H.M. Alkhalifah, W.N. Hozzein, *ACS Omega* **8**, (2023)
44. M. Gadewar, G.K. Prashanth, M. Ravindra Babu, M.S. Dileep, P. Prashanth, S. Rao, M. Mahadevaswamy, M. Kumar Ghosh, N. Singh, S.K. Mandotra, A. Chauhan, S. Rustagi, R. Yogi, S. Chinnam, B. Ali, S. Ercisli, E. Orhan, *J. Saudi Chem. Soc.* **28**, 101774 (2024)
45. I. Kim, K. Viswanathan, G. Kasi, S. Thanakkasaranee, K. Sadeghi, J. Seo, *Food Reviews Int.* **38**, (2022)
46. N. Farid, A. Waheed, S. Motwani, *Heliyon* **9**, (2023)
47. Y. Zhu, S. Zhang, *Front. Microbiol.* **11**, (2020)
48. S. Suriyaprom, P. Mosoni, S. Leroy, T. Kaewkod, M. Desvaux, Y. Tragoolpua, *Antioxidants* **11**, (2022)
49. A. Sirelkhatim, S. Mahmud, A. Seeni, N.H.M. Kaus, L.C. Ann, S.K.M. Bakhori, H. Hasan, D. Mohamad, *Nanomicro Lett.* **7**, 219 (2015)
50. S.E. Jin, H.E. Jin, *Nanomaterials* **11**, (2021)
51. S. Shaikh, N. Nazam, S.M.D. Rizvi, K. Ahmad, M.H. Baig, E.J. Lee, I. Choi, *Int. J. Mol. Sci.* **20**, (2019)
52. J. Bai, X. Gongsun, L. Xue, M.M. Zangeneh, *J. Exp. Nanosci.* **16**, (2021)
53. M. Jayanetti, C. Thambiliyagodage, H. Liyanaarachchi, G. Ekanayake, A. Mendis, L. Usgodaarachchi, *Sci. Rep.* **14**, 1293 (2024)
54. S. Jiang, K. Lin, M. Cai, *Front. Chem.* **8**, (2020)
55. S.S. Naser, B. Ghosh, F.Z. Simnani, D. Singh, A. Choudhury, A. Nandi, A. Sinha, E. Jha, P.K. Panda, M. Suar, S.K. Verma, *J. Nanotheranostics* **4**, (2023)
56. M.T. Yassin, A.A. Al-Askar, K. Maniah, F.O. Al-Otibi, *Cryst. (Basel)* **12**, (2022)
57. V. Jayakar, V. Lokapur, B.R. Nityasree, R.K. Chalannavar, L.D. Lasrado, M. Shantaram, *Biomed. (India)* **41**, (2021)
58. J. Gaur, S. Kumar, M. Pal, H. Kaur, K.M. Batoo, J.O. Momoh, Supreet, *Hybrid. Adv.* **5**, 100128 (2024)
59. H.H. Basri, R.A. Talib, R. Sukor, S.H. Othman, H. Ariffin, *Nanomaterials* **10**, (2020)
60. C. Chikkanayakanahalli Paramesh, G. Halligudra, V. Gangaraju, J.B. Sriramoju, M. Shastri, H. Kachigere, B.P. Habbanakuppe, D.D. Rangappa, R. Kanchugarakoppal, Subbegowda, and P. Doddakunche Shivaramu, *Results in Surfaces and Interfaces* **3**, 100005 (2021)
61. G. Halligudra, C.C. Paramesh, R. Mudike, M. Ningegowda, D. Rangappa, P.D. Shivaramu, *ACS Omega.* **6**, 34416 (2021)
62. R. Mudike, C. Sabbanaahalli, J.B. Sriramoju, A. Bheemaraju, G. Halligudra, M. Muniyappa, M.P. Narayanaswamy, A.K. CS, P.D. Shivaramu, D. Rangappa, *Mater. Res. Bull.* **146**, 111606 (2022)
63. C.C. Paramesh, G. Halligudra, M. Muniyappa, M. Shetty, K.K. Somashekharappa, D. Rangappa, K.S. Rangappa, P.D. Shivaramu, *Ceram. Int.* **47**, 14750 (2021)

64. G. Halligudra, C.C. Paramesh, R. Gururaj, A. Giridasappa, C. Sabbanahalli, A.K. Channapillekoppalu, A.K. Siddegowda, D. Madikere Raghunathareddy, Rangappa, and P. Doddakunche Shivaramu, *Ceram Int* **48**, (2022)
65. G. Halligudra, C. Chikkanayakanahalli Paramesh, M. Shetty, H. Kachigere Bhadracharya, V. Kambappa, A.K. Channapillekoppalu Siddegowda, D. Rangappa, R. Kanchugarakoppal, Subbegowda, and P. Doddakunche Shivaramu, *Journal of the Iranian Chemical Society* **1** (2022)
66. G. Halligudra, P.D. Shivaramu, C.C. Paramesh, K. Roy, C. Sabbanahalli, M. P. N., V. K., A. K. C. S., and, D. Rangappa, *J. Inorg. Organomet. Polym. Mater.* (2024)
67. J.B. Sriramoju, C.C. Paramesh, G. Halligudra, D. Rangappa, P.D. Shivaramu, *Photocatalytic Systems by Design* (Elsevier, 2021), pp. 503–536
68. D. Singh, D. Rawat, Isha, *Bioresour Bioprocess.* **3**, (2016)
69. B. V. N. S.; K. M. R. ; T. T. ; R. O. M. F. ; N. K. M. Kumar, *Pharma Sci. Monit.* **2**, 59 (2011)
70. P. Prerna, N. Vasudeva, *Indian J. Nat. Prod. Resour.* **6**, (2015)
71. P. Manikanta, *Int. J. Univers. Pharm. Biosci.* **3**, 206 (2014)
72. C.A. Nayak, N.K. Rastogi, K.S.M.S. Raghavarao, *Int. J. Food Prop.* **13**, (2010)
73. S.A. Lamture, D.S. Bhatkhande, *Ind. J. Sci. Res. Tech.* **2**, (2014)
74. V. Azimian-Zavareh, G. Hossein, E. Janzamin, *Indian J. Pharmacol.* **44**, (2012)
75. R.P. Thylur, S. Senthivinayagam, E.M. Campbell, V. Rangasamy, N. Thorenoor, G. Sondarva, S. Mehrotra, P. Mishra, E. Zook, P.T. Le, A. Rana, B. Rana, *J. Biol. Chem.* **286**, (2011)
76. A. Narayana, S.A. Bhat, A. Fathima, S.V. Lokesh, S.G. Surya, C.V. Yelamaggad, *RSC Adv.* **10**, (2020)

**Publisher's Note** Springer Nature remains neutral with regard to jurisdictional claims in published maps and institutional affiliations.

Springer Nature or its licensor (e.g. a society or other partner) holds exclusive rights to this article under a publishing agreement with the author(s) or other rightsholder(s); author self-archiving of the accepted manuscript version of this article is solely governed by the terms of such publishing agreement and applicable law.